Ocean Sci. Discuss., 11, 2569–2606, 2014
www.ocean-sci-discuss.net/11/2569/2014/
doi:10.5194/osd-11-2569-2014

Ocean Science
Discussions
Open Access

Water level oscillations in Monterey Bay and Harbor

J. Park, W. Sweet, and R. Heitsenrether

NOAA, 1305 East West Hwy, Silver Spring, MD, USA

Received: 13 October 2014 – Accepted: 28 October 2014 – Published: 20 November 2014

Correspondence to: J. Park (joseph.park@noaa.gov)

Published by Copernicus Publications on behalf of the European Geosciences Union.

Abstract

Seiches are normal modes of water bodies responding to geophysical forcings with potential to significantly impact ecology and maritime operations. Analysis of high-frequency (1 Hz) water level data in Monterey California identifies Harbor modes between 10 and 120 s that are attributed with specific geographic features. It found that modal amplitude modulation arises from cross-modal interaction and that offshore wave energy is a primary driver of these modes. Synchronous coupling between modes is observed to significantly impact dynamic water levels. At lower frequencies between 15 and 60 min modes are independent of offshore wave energy, yet are continuously present. This is unexpected since seiches normally dissipate after cessation of the driving force, indicating an unknown forcing. Spectral and kinematic estimates of these low frequency oscillations supports the idea that a persistent anticyclonic mesoscale gyre adjacent to the Bay is a potential mode driver, while discounting other sources.

1 Introduction

Bounded physical systems support normal modes. This is true in quantum mechanical, astronomical, and terrestrial systems such as harbors and bays, and owing to the central role that harbors play in human endeavors there is a rich history analyzing resonant modes of bays and harbors (seiches), see for example Darwin (1899); Chrystal (1906); AMS (1903, 1906).

Monterey Bay California is a dynamic and ecologically rich system influenced by Monterey Submarine Canyon, the California Current, seasonal upwelling, and inshore countercurrents (California undercurrent, Davidson current). Monterey Submarine Canyon is the prominent bathymetric feature where tidally coherent internal waves are nearly an order of magnitude stronger than the open ocean with the most intense waves characterized as bores (Kunze et al., 2002; Key, 1999; Petruncio et al., 1998), and where hydrodynamic mixing (turbulent kinetic energy dissipation) reaches three

OSD
11, 2569–2606, 2014

orders of magnitude greater than the open ocean (Carter and Gregg, 2002). Interaction of the regional coastline and bathymetry with the California Current establishes a persistent anticyclonic mesoscale vortex adjacent to the Bay that is readily observed in satellite ocean surface temperature images (Strub et al., 1991; Rosenfeld et al., 1994) and in high resolution hydrodynamic models (Tseng et al., 2005, 2012; Tseng and Breaker, 2007). Upwelling driven by local wind forcing interacts with this gyre resulting in a bifurcated flow of upwelled water with one branch advected northward near Point Año Nuevo just north of the Bay, and the other directed equatorward along the outside edge of the Bay (Rosenfeld et al., 1994).

The Bay supports commercial fishing, diving and marine recreation industries serviced from harbors in Monterey, Moss Landing and Santa Cruz. Water level oscillations in the Bay and harbors, along with their associated hydraulic currents, play a significant role in the safety and operation of these interests, and, from an oceanographic perspective Breaker et al. (2008) have posed an open question regarding the continuous forcing of these modes. That is, seiches are normally excited by transient forcings such as seismic or meteorological events, then tend to lose energy and dissipate, however, modal oscillations in Monterey Bay are observed to be continuously present.

The seminal study of Bay modes was contributed by Wilson et al. (1965) who applied analytical and numerical models of increasing sophistication to characterize the oscillations. While some of the numerical results were unsatisfying, the breadth and depth of the analysis was pioneering, and many of the fundamental results quantifying Bay modes have been corroborated over ensuing decades. Wilson et al. assumed that "the surge phenomenon in Monterey Harbor is the consequence of surf-beats or of genuine long-period waves", concluding that the latter was likely the cause, and it is notable that previous studies did indicate the continuous presence of oscillations. For example, Forston et al. (1949) analyzed a six month wave gauge record and found that 8–22 s period waves were present nearly 100 % of the time, and Raines (1967) examined a three year tide gauge record finding that "shorter waves (1.5–2 min) are recorded almost continuously", however, we believe that Breaker et al. (2008) were

OSD
11, 2569–2606, 2014

the first to conclusively observe that long period Bay-wide oscillations are effectively stationary and to question their genesis.

Breaker et al. (2010) contributed a comprehensive review and analysis of Monterey Bay oscillations, and based on measurements over an 18 month period determined primary Bay modes at the Monterey tide gauge of 55.9, 36.7, 27.4, 21.8, 18.4 and 16.5 min, broadly consistent with the work of Wilson et al. There is general agreement that the 55.9 min mode represents the fundamental longitudinal mode (north–south), while the 36.7 min harmonic is attributed to the primary transverse mode (east–west). It is also accepted that Monterey Submarine Canyon acts to decouple the Bay into two weakly-coupled oscillators, one north of the canyon and one south. Regarding Monterey Harbor, estimates of modal periods are more variable with most sources suggesting periods of 1–2 to 13.3 min, and several making specific mention of 9–10 min.

Previous observational studies (reviewed in Breaker et al., 2010) used water level data sampled at (or averaged to) daily, hourly, six, four or 1 min intervals such that periods below several minutes are not resolved. Here, we examine a 63 day record of 1 Hz water level recorded at the National Oceanic and Atmospheric Administration (NOAA) Monterey tide gauge allowing spectral characterization of water level variance to periods as short as 2 s. This high-resolution data is used to quantify and attribute water level oscillation modes in Monterey Bay and Harbor with physical processes and boundary conditions. We also analyze a 17.8 year record of 6 min water levels to characterize modes associated with Bay-wide resonances, which to our knowledge is the longest continuous record of water levels to be analyzed for modal oscillations in Monterey Bay, and we examine potential mode drivers of the Bay-wide oscillations.

2 Length scales

The dispersion relation for surface gravity waves dictates length scales corresponding with water depth and oscillation period (resolved from spectral analysis), and we characterize water level oscillations as belonging to Bay, Bight or Harbor modes ac-

OSD
11, 2569–2606, 2014

cording to spatial scales appropriate to each domain as shown in Table 1. We define Harbor oscillations as modes with periods less than 180 s and wavelengths less than 1 km matching spatial scales within the breakwater of Monterey Harbor (Figs. 1 and 4). Modes with periods between 2 and 15 min and length scales between 2 and 10 km are considered Bight modes associated with resonances between Point Pinos at the tip of Monterey Peninsula and the eastern shore of the Bay. Bay modes have periods longer than 15 min and scales from 10 to 40 km. The lowest frequency Bay modes correspond to the longitudinal and transverse lengths of the Bay.

3 Observations

Observations consist of a 63 day record (14 September through 29 November 2013) of 1 Hz water level from a microwave ranging sensor located at the NOAA tide station located on Monterey Municipal Wharf #2 (NOAA, 2014a), a 17.8 year record of 6 min water levels (23 August 1996–30 June 2014) from an acoustic ranging tide gauge located 4 m shoreward of the microwave sensor, and offshore wave height estimated every 30 min from the Coastal Data Information Program (CDIP) buoy located above Monterey Submarine Canyon (CDIP, 2014). Gauge locations are shown in Fig. 1.

Since the Bay and Harbor oscillations are at much higher frequencies than the tides, we remove the tidal signal from the 1 Hz water level and deal with the water level nontide residual (NTR). The tidal response is obtained from standard NOAA tidal predictions at the Monterey tide gauge derived from 37 harmonic constituents over the tidal datum epoch of 1983 to 2001 (NOAA, 2014b).

Continuous availability of the 1 Hz data was not achieved, resulting in five segments of lengths 12.1, 12.3, 14.3, 10.5 and 14.1 days as shown in Fig. 2 exhibiting a relationship between nontide residual and offshore wave height. Since the magnitude of nontide residual is a measure of the variance of the water level minus tide, it should be related to the canonical definition of significant wave height: $H_{m0} = 4\sigma$, where H_{m0} is the zeroth-moment of the water elevation spectrum and σ the standard deviation

OSD
11, 2569–2606, 2014

of water level. However here, the water level variance and the significant wave height are not collocated so that the canonical relationship is not expected to be realized. Nonetheless, it is worth noting that water level variance estimates from tide gauges are robustly related to wave height and do have potential as proxies of wave height estimates (Parke and Gill, 1995; IOOS, 2009; Park et al., 2014).

4 Oscillations in Monterey Harbor

Figure 3 presents 1 Hz water level data over 14 days of November 2013, the corresponding spectrogram of 1 Hz nontide residual computed with 60 min windows and 50 % overlap, and a power spectral density (PSD) estimate of the 14 day, 1 Hz nontide residual. Power spectral densities are estimated by periodogram with a split cosine bell taper and modified-Daniell smoother (Bloomfield, 1976). The PSD indicates that dominant Harbor energy is found at periods of 112, 60, 41, 31, 16, 12 s and are marked with vertical dashed lines. Bight modes are also identified with dash-dot lines (10.1, 9.0 and 4.2 min), and Bay modes with dashed lines (55.9, 36.7, 27.4, 21.8, 18.4 and 16.5 min). Bight and Bay modes are discussed in a following section.

4.1 Harbor modes

Harbor modes are typified by smooth broad peaks in the PSD, suggesting that for a specific Harbor component there are multiple harmonic oscillators closely grouped in wavenumber space leading us to expect that there will be a nearly continuous range of spatial scales contributing to these modes. In addition to the broad spectral peak centered on 112 s, there are also distinct spectral lines near 112 s indicating specific resonant scales. The spectrogram reveals a time-dependent intensity of Harbor modes, for example the generally low amplitudes around 25 November and high amplitudes following 27 November. Referring to Fig. 2 suggests that offshore wave height influences Harbor amplitudes. Another interesting feature is the frequency modulation (FM) of

OSD
11, 2569–2606, 2014

modes coherent with the tidal signal. We believe that this frequency modulation arises from the changing water depth and shoreline profile as mean water level rises and falls such that different length scales for surface waves are realized. These spectral features are representative of all 1 Hz data.

Figure 4 shows a chart of the Harbor with circles of radius $\lambda/2$ centered on the location of the water level gauge where λ is governed by the dispersion relation at a water depth of 7.5 m for mode periods identified in Fig. 3. The highest frequency modes with periods of 12 and 16 s are not depicted in Fig. 4, they are associated with reflections from wharf infrastructure. The 31 s mode matches the length scale for reflections from a landing platform south of the gauge, the 41 s mode is attributed to a standing wave between the gauge and the breakwater protecting the mooring docks, while the 60 s mode matches a spatial resonance between the gauge and Wharf #1.

The 112 s mode is the dominant Harbor mode containing multiple resonances close in wavenumber sustained by standing waves between the gauge and the rocky coast to the west, the mooring docks to the northwest and the breakwater to the north. Also shown in Fig. 4 are spatial scales corresponding to resonances at 84 and 96 s which we attribute to reflections from the breakwater to the north.

4.2 Wave height

To asses the wave dependence of Harbor mode amplitudes Fig. 5 presents NTR PSD estimates during three 2 h periods when offshore wave height was increasing. With a significant wave height of 0.8 m (dominant period T_s = 5.9 s) the characteristic Harbor modes are broadly observed with the 60 s period reflection from the breakwater well resolved. As significant wave height grows from 0.8 to 1.1 m most of the energy increase is contained in the band between 80 and 300 s suggesting that it is a combination of growing reflections from the rocky shore to the west, the breakwater to the north and a Bight mode contributing to increased NTR variance. When offshore wave height reaches 2.4 m (T_s = 12.5 s) there is a significant increase in energy at all modes, and a conspicuous broadening of the 80 to 120 s resonances suggesting that a rich set

OSD
11, 2569–2606, 2014

of closely spaced modes is being driven. We also note that spectral shapes are essentially invariant as offshore waves transition from periods of 6 to 12 s but the amplitudes increase, indicating that these modes are generated by local resonances in the Harbor forced by offshore wave energy, but independent of wave period.

To quantify the amplitude dependence of offshore wave height on Harbor and Bay oscillations we regress PSD amplitudes of the dominant Harbor and Bay modes (112 s and 36.7 min respectively) against offshore significant wave height (H_s):

$$\mathrm{PSD_M} = \alpha H_s + \beta H_s^{1/2} \quad (1)$$

where $\mathrm{PSD_M}$ are 1 Hz NTR PSD amplitudes in dB of the 36.7 min or 112 s modes over a 24 h sliding window advanced in 2 h increments over all data. Figure 6 plots the data and model fits indicating that the Harbor mode responds to offshore wave amplitude with nonlinear growth ($r^2 = 0.70$), while the Bay mode has no such dependence ($r^2 = 0.03$).

4.3 Wave direction

To examine offshore wave direction in the forcing of Harbor modes, Fig. 7 plots NTR PSD estimates from two periods when offshore significant wave heights were small (0.5–0.7 m), but the dominant wave direction was either west (250° N) or northwest (295° N).

With the exception of the 15 s resonance, Harbor modes are significantly enhanced when low amplitude waves are arriving from the northwest instead of the west. This is consistent with the wave refraction analysis presented by Wilson et al. (1965) indicating that wave energy from the west is less efficiently refracted into the Harbor than waves from the northwest. When waves are larger a comparison of NTR spectra finds that wave direction has a smaller influence, although some specific modes may be selectively enhanced.

OSD
11, 2569–2606, 2014

4.4 Tidal phase

Spectrograms of 1 Hz data indicate that tidal phase serves to modulate the frequency of Harbor modes. To examine this we selected a period with minimum offshore wave height covering a semidiurnal tidal cycle (25 November 04:30 to 14:00 UTC) and compare NTR PSD estimates over 2 h periods centered on the low and high water tidal phase as shown in Fig. 8. There is a clear shift from longer to shorter periods at high water in relation to low water supporting the idea that water depth and associated shoreline characteristics influence the modal structure of the Harbor. We also note a general increase in amplitude at high water.

4.5 Dynamic mode response

The dynamic characteristics of Harbor modes can be assessed by decomposing the 1 Hz nontide residuals into components capturing temporal variations at different timescales with a maximal overlap discrete wavelet transform (MODWT, Percival and Walden, 2006). The MODWT is defined in Appendix A and we employ an eleven level ($J = 11$) transform based on the least asymmetric mother wavelet (LA8). Approximate temporal scales for the wavelet levels are listed in Table 2.

Figure 9 plots the MODWT decomposition two of the 2 h periods shown in Fig. 5. The bottom panel of each plot shows the NTR time series with panels above in ascending order plotting the wavelet coefficients for each level of increasing timescale. With offshore significant wave heights of 0.8 m (0–2000 s in Fig. 9a) the NTR energy is fairly evenly distributed between the W_3, W_4, W_5, W_6, W_{10} and W_{11} levels corresponding to temporal scales of 15, 31, 59, 99, 900 and 1800 s. As waves grow from 0.8 to 1.1 m (3000–7000 s in Fig. 9a) the W_6 and W_7 levels exhibit the emergence of oscillatory modes at timescales of 96 and 126 s, consistent with the spectral perspective shown in Fig. 5. When waves have grown to 2.4 m we find in Fig. 9b that the W_5, W_6 and W_7 timescales (58, 101, 117 s) are dominating the NTR energy, again consistent with the Fourier decomposition in Fig. 5. The same general behavior with the emer-

OSD
11, 2569–2606, 2014

gence, growth and dominance of the 50 to 120 s modes in Monterey Harbor during wave events is robustly observed.

An interesting feature of these primary Harbor modes (W_5, W_6 and W_7) is their temporal amplitude modulation (AM). These AM effects are generally not synchronous across levels, and appear to have modulation periods in the neighborhood of 20 min. These periods are not representative of the Bay or Bight modes previously identified, and their non-synchronous nature suggests that they are not forced by a unitary driver, e.g. long period waves propagating from offshore. However, we previously noted the broad spectral nature of the Harbor modes indicative of multiple harmonic oscillators closely spaced in frequency/wavenumber and this leads us to speculate that the AM arises from superposition of closely spaced modes in frequency space. To test this hypothesis we select 10 spectral amplitudes from the NTR PSD with 2.4 m wave height from Fig. 5 at periods of 58, 83, 94, 97, 100, 104, 107, 112 116, and 209 s, and create a reconstruction from these components with a harmonic superposition:

$$R = \sum_i A_i \sin(\omega_i t) \tag{2}$$

where A_i is the NTR spectral amplitude and ω_i the frequency. This reconstruction is compared to the W_6 level in Fig. 10 where the envelope has been plotted for each time series. Qualitatively, the overall AM behavior of the reconstructed superposition and the actual mode is similar, leading to the suggestion that it is cross-modal interference of closely spaced Harbor modes resulting in the AM of specific resonances. Although the AM envelopes are generally not synchronous, there is nothing precluding such a synchronization and in Fig. 11 we present evidence of such a synchronization between the W_6 and W_7 levels suggesting that when modes synchronize their impact on the overall NTR can be significant.

OSD
11, 2569–2606, 2014

5 Oscillations in Monterey Bay

The Bay modes are clearly identified in 1 Hz spectra (Fig. 3) and we estimate their water level amplitudes over the 63 day period by computing mean PSD amplitudes over all 1 Hz data over a sliding window of 24 h advanced in 2 h increments. The modes are ranked in terms of decreasing amplitude in Table 3 indicating that the 36.7 min mode exhibits the highest average power. Improved spectral resolution is afforded by a longer record and Fig. 12 presents a spectrogram and PSD of a 17.8 year record of 6 min water level data. Spectrogram PSDs are from records of 2048 points (8.53 days) with 50 % overlap. The two dominant features are the annual occurrence of increased broadband variance from winter storms (vertical bands), and the continuously present energy at the Bay periods quantified by Breaker et al. (2010).

The PSD reveals that the 36.7 min transverse Bay mode is not only the most energetic, but is actually a series of closely-spaced modes. The dominance of this mode suggests that the primary transverse Bay resonance is the mode most directly coupled to the unknown continuous forcing of Bay oscillations. The 27.4 min mode exhibits a high Q factor indicating a resonance highly tuned to the source. The spatial harmonics of this mode correspond to a partitioning of the Bay into thirds (Breaker et al., 2010; Wilson et al., 1965) with northern, central (canyon) and southern components suggesting that this mode is efficiently tuned to the decoupling of the southern and northern parts of Bay by the canyon, whereas the fundamental longitudinal mode (55.9 min) is not.

5.1 Mode forcing

Breaker et al. (2010) considered six physical mechanisms as prospective forcings for continuous oscillations of the Bay:

1. edge waves
2. Long period surface waves

OSD
11, 2569–2606, 2014

3. Sea breeze
4. Internal waves
5. Microseisms
6. Small scale turbulence

and noted that first three are not likely to be continuously present, and so are not consistent with the observation of persistent oscillations. Tidally synchronous internal waves have been observed propagating up the submarine canyon and episodically transition to bores (Key, 1999; Kunze et al., 2002; Carter and Gregg, 2002), their tidal coupling suggests a continuous presence and potential mode forcing. Microseisms are an appealing candidate due their omnipresence (Kedar et al., 2008), however, it was speculated that their energy was insufficient at the Bay frequencies to drive the oscillations. Breaker et al. (2010) also discounted small scale turbulence on the basis of its intermittent nature. These arguments are based primarily on temporal persistence, however, we offer an alternative perspective based on kinematic energy scales.

Under the assumption that the 36.7 min mode is the directly forced fundamental mode, we can ask questions regarding its observed amplitude and spectral resonance to grossly estimate the energy required to sustain it. Table 3 indicates that the RMS water level deviation of this mode at the Monterey tide gauge is $h_M = 0.341$ m. Neglecting the effect of shoaling on wavelength, a cosine profile with $\lambda/2 = 26.7$ km (Table 1) approximates the cross-shore elevation of the mode with a profile area of $A_M = 9104\,m^2$. Breaker et al. (2010) assessed spatial harmonics of Bay modes with a regional ocean modeling system (ROMS) implementation (Shchepetkin and McWilliams, 2005) providing an estimate of the alongshore profile of this mode. They found strong harmonic response over the majority of the eastern Bay shoreline with a damped response in an area north of the submarine canyon. Based on this, we estimate that approximately 70 % of the shoreline responds to this mode. In the spirit of our gross estimate, we assume the alongshore spatial dimension of the mode to be $L_A \approx 0.7 \times 40\,km = 28\,km$.

OSD
11, 2569–2606, 2014

Combining this with the cross-shore elevation area we arrive at an estimate of the volume of water displaced by this mode of $V_M = L_A A_M \approx 258\,\mathrm{Mm}^3$. The energy to move this mass is equivalent to the work performed to change the potential energy of the mass in the gravitional field, and we estimate the energy of the mode as $E_M = \rho V_M h_M g \approx 894.75\,\mathrm{GJ}$, or an average power of 406 MW over the 36.7 min modal period. Obviously this leading-order value does not incorporate dissipation and momentum, terms that we ignore in all subsequent energy estimates.

The ratio of energy stored in the mode resonance to energy supplied driving the resonance is the Q factor. If Q is large (the resonance signal-to-noise ratio is high), then it may be estimated from the power spectrum: $Q = f_M/\Delta f$, where f_M is the mode resonant frequency and Δf the −3 dB (half power) bandwidth of the mode. We observe signal-to-noise ratios routinely exceeding 5 dB at the Bay modes (Figs. 3 and 12) and use PSD estimates based on 120 h records of 1 Hz NTR (95 % CI 2.6 dB) advanced in 4 h increments to find a mean $\Delta f = 5.86^{-5}$ Hz and an estimate of $Q = 7.74$ for the 36.7 min mode. This implies that within the gross level of estimation which we are engaged, the driving energy for the 36.7 min mode is roughly $894.75/7.75 \approx 115.5$ GJ or a power consumption of 52.4 MW. We will compare this forcing to estimates of energy available from prospective mode drivers in the following sections.

5.1.1 Microseisms

Microseisms are pressure (acoustic) waves primarily generated by nonlinear wave-wave interactions on the ocean surface. They radiate into the atmosphere where they are globally detected as microbaroms (Waxler and Gilbert, 2006), into the water column as acoustic modes, and couple into the seafloor where they travel as Rayleigh/Stonely waves presenting a global seismic signature (Webb and Cox, 1986). One can estimate deep water microseismic energy by considering the acoustic intensity of a plane wave incident on the seafloor $I_A = P^2/Z$ where P is the pressure and Z the acoustic impedance. In the linear regime the characteristic acoustic impedance of a medium is $Z_0 = \rho c$ where ρ is the density and c the sound speed, which in the case of seawa-

OSD
11, 2569–2606, 2014

ter is approximately $Z_0 \approx 1.5^6\,\mathrm{N\,s\,m^{-3}}$. Spectral amplitudes of the microseism peak at deep water seafloor sites were found by Webb and Cox (1986) to be approximately $5000\,\mathrm{Pa^2\,Hz^{-1}}$, giving an intensity of $I_A \approx 5^{-3}\,\mathrm{W\,m^{-2}}$. Assuming a source generation region of radius 100 km the total power is 157 MW.

This energy is efficiently converted into seismic Rayleigh waves or ocean acoustic modes (Hasselmann, 1963), and these waves can propagate with small attenuation coefficients over large distances suggesting that microseismic energy is of sufficient magnitude to couple to Bay resonances. However, Bromirski and Duennebier (2002) demonstrate that coastal zone microseismic energy is dominated by local wave reflections from coasts, not deep water arrivals as propagation from deep to shallow water is inhibited by the changing seismic waveguide as refraction of the Rayleigh modes significantly reduces energy reaching the coastal zone (Hasselmann, 1963). Bromirski and Duennebier (2002) found coastal zone pressures of approximately $70\,\mathrm{Pa^2\,Hz^{-1}}$, which under the same assumptions as the deep water case gives a total power of 2.2 MW, insufficient to drive the fundamental Bay mode. Not only is the estimated energy insufficient, microseismic energy is distributed around periods of 5 to 7 s, more than two orders of magnitude shorter than the dominant Bay mode, and we conclude that microseisms are not a likely driving mechanism for the continuous Bay oscillations.

5.1.2 Internal waves

Kunze et al. (2002) observed that internal waves in Monterey Canyon are nearly an order of magnitude more energetic than in the open ocean and are tidally-locked to M_2. Mean horizontal energy fluxes are steered by canyon bathymetry and are predominantly up canyon with depth integrated fluxes of $5\,\mathrm{kW\,m^{-1}}$ at the mouth diminishing to $\pm 1\,\mathrm{kW\,m^{-1}}$ near the head (Moss Landing), although the internal wave field is highly anisotropic with with evidence of both sources and sinks along the canyon. Particularly energetic fluxes have been characterized as bores with with peak currents of $55\,\mathrm{cm\,s^{-1}}$ and 2 h averages exceeding $30\,\mathrm{cm\,s^{-1}}$ (Key, 1999). Carter and Gregg (2002) quantified

OSD
11, 2569–2606, 2014

turbulent kinetic energy dissipation finding that the turbulence is primarily in a stratified turbulent layer (STL) along the canyon floor and is thickest on the canyon axis. Time averaged values of STL thickness and dissipation were estimated to be 135 m and $\overline{\varepsilon} = 1.36^{-6}\,\mathrm{W\,kg^{-1}}$.

Both Kunze et al. (2002) and Carter and Gregg (2002) compared mean internal wave energy flux with dissipation rates tentatively concluding that most of the along-canyon internal energy is dissipated as turbulence, although Carter and Gregg (2002) noted that "large error estimates suggest this agreement is fortuitous". A gross estimate of the internal tide energy can be made from a mean value of energy flux: $2\,\mathrm{kW\,m^{-1}}$ (Kunze et al., 2002), which for a 20 km length of canyon gives $P_\mathrm{I} \approx 40$ MW (20 km corresponds to the length of Canyon from the head over which there is a primarily a single channel, is approximately equal to the length of the primary transverse mode, and is the length used by Carter and Gregg (2002) in their global estimates of canyon dissipation). An estimate of the dissipation over this 20 km section with a mean STL height of 135 m and width of 4 km ($V_\mathrm{STL} = 10.8\,\mathrm{Gm^3}$) gives: $P_\mathrm{T} = \rho V_\mathrm{STL} \overline{\varepsilon} \approx 15.1$ MW.

Even if these gross estimates of internal wave energy and dissipation, which ignore the well documented finescale sink/source and spatial variability are only accurate to a factor of 2, the residual energy rate $P_\mathrm{I} - P_\mathrm{T} = 40 - 15 = 25$ MW is insufficient to sustain our estimate of the fundamental mode (52.4 MW).

5.1.3 Mesoscale eddy

A potential energy source that to the authors knowledge has not been considered as a mode driver is the persistent mesoscale anticyclonic gyre offshore Monterey Bay. The gyre is nominally 50–70 km in diameter and models suggest that it extends from the surface to at least 600 m in depth with instantaneous velocities of $70\,\mathrm{cm\,s^{-1}}$ near the surface and $30\,\mathrm{cm\,s^{-1}}$ at depth (Tseng and Breaker, 2007; Tseng et al., 2012). The gyre supports a persistent elevated dome of sea surface height (SSH) rising approximately 10–12 cm above the coastal levels along the eastern shore of the Bay (Tseng et al., 2012).

OSD
11, 2569–2606, 2014

The potential energy of this dome with respect to the coast can be estimated by assuming the dome has a cosine-bell profile from the center with $\lambda/2 \approx 30\,\mathrm{km}$. Taking the height of the dome to be $h_G = 10\,\mathrm{cm}$, the dome volume is $V_G = 2\pi\int_0^{\lambda/2}[h_G x + h_G x\cos(kx)]\,\mathrm{d}x = 168\,\mathrm{Mm}^3$ where $k = 2\pi/\lambda$. The potential energy of this mass is $E_G = \rho V_G g \frac{h_G}{\sqrt{2}} = 120.7\,\mathrm{GJ}$, which is comparable with the 115.5 GJ estimated to sustain the 36.7 min fundamental mode. However, even though the geostrophic balance of the gyre will fluctuate due to wind stress and dynamics of gyre interaction with the California Current, it is unlikely that the geostrophic balance will fluctuate by its full amplitude on timescales of 30 min allowing this mass of water to relax and propagate as a wave.

The kinetic energy of the equatorward portion of the gyre can be estimated from the cross-sectional flow of the gyre, which from the model of Tseng and Breaker (2007) during a weak flow regime (April) can be represented as a velocity of $u = 5\,\mathrm{cm\,s}^{-1}$ from a depth of at least 200 to 600 m over a width of 30 km. A 30 km long section of this flow (corresponding to the length of the equatorward portion of the gyre just offshore the Bay) would have a kinetic energy of $E_K = \frac{1}{2}\rho V_K u^2 = 465.8\,\mathrm{GJ}$, so there appears to be sufficient energy in the jet offshore the Bay to sustain the fundamental mode, but it is not clear how a portion of this energy would couple into the mode.

One possibility is that the shear interface between the jet and deeper water generate Kelvin-Helmholtz instabilities to drive the fundamental mode. With the assumption of two stratified water masses of density ρ_1 and ρ_2 and mean velocities U_1 and U_2, the minimum horizontal wavenumber of instabilities can be found from a dispersion relation of the unsteady Bernoulli equation (Kundu, 1990) as:

$$k_{\min} < \frac{g\left(\rho_2^2 - \rho_1^2\right)}{\rho_1\rho_2(U_2 - U_1)^2}. \tag{3}$$

To apply this we assume that the upper water mass is the warmer, fresher water of the California Current gyre (ρ_1, U_1) and the lower layer the colder, saltier deep water

OSD
11, 2569–2606, 2014

(ρ_2, U_2) where values of $\rho_1 = 1026.70\,\mathrm{kg\,m^{-3}}$ and $\rho_2 = 1026.97\,\mathrm{kg\,m^{-3}}$ are mean values from the surface to a depth of 200 m at offshore and canyon locations computed from temperature and salinities reported in Fig. 13 of Rosenfeld et al. (1994) using the method of Gill (1982). The resultant maximum wavelengths over the range of velocity differences suggested by Tseng and Breaker (2007) (30–70 $\mathrm{cm\,s^{-1}}$) indicate that instabilities with length scales of several hundred meters are possible. However, these length scales are much shorter than the characteristic scale of the 36.7 min fundamental Bay mode (26.7 km), and it seems unlikely that even coherent trains of such instabilities could effectively drive the fundamental mode.

Finally, we examined whether there was a relation between the seasonal upwelling and mode response. Upwelling in the Bay typically peaks in Spring/Summer (April/May) introducing a tongue of upwelled water between the gyre and the outside edge of the Bay. It was assumed that if the Bay modes are driven by the gyre, then upwelling which might partially decouple the Bay from the gyre, could have an impact on the Bay mode amplitudes. We compared PSD estimates of the 6 min data averaged over 17 years for April and May with PSD estimates from September and October but found no statistically significant differences. To the extent that upwelling was expressed in the April and May data we find no evidence to support the idea that it changes the oscillating modes.

6 Conclusions

Monterey Bay is an intensely studied oceanic body with the Naval Postgraduate School, Moss Landing Marine Laboratories, Hopkins Marine Station and Monterey Bay Aquarium Research Institute providing decades of physical oceanographic research. Water level oscillations in the Bay have been studied since at least the late 1940s, yet it seems that Breaker et al. (2008) were the first to notice that Bay-wide oscillations are continuously present. Based on a 17.8 year record of water levels at the NOAA tide station we substantiate their observation and validate the accuracy of oscillation periods of the six

OSD
11, 2569–2606, 2014

primary Bay modes determined by Breaker et al. (2010). Amplitudes of the Bay modes indicate that the fundamental transverse mode (36.7 min) is the mode that is most directly driven by the unknown source. Kinematics of this oscillation coupled with the resonance amplitude lead us to estimate that a power source of roughly 52.4 MW drives this mode. Comparison of this energy rate to prospective forcings from microseisms, internal waves and the associated turbulence indicate that neither of these mechanisms have sufficient power to sustain the mode. We also find that surface waves are not coherently related to the Bay modes.

A potential mode driver is the anticyclonic mesoscale gyre situated just offshore the Bay. The potential and kinetic energy it contains are sufficient to sustain the fundamental mode, however, we find that turbulent instabilities such as Kelvin-Helmholtz waves generated in the shear interface of the gyre do not have spatial scales consistent with the fundamental mode. It is intriguing to note that the nodal line of the fundamental transverse mode would be located roughly $\lambda/2 = 26.7$ km from the eastern shore, corresponding roughly to the eastern edge of the gyre. It would seem a peculiar circumstance if this spatial arrangement along with the potential and kinetic energy scales of the gyre were merely coincidental to the continuous harmonic driver of Bay modes, but presently we cannot conceptualize a supportable mechanism for such a coupling. While the present study is purely observational, high-resolution non-hydrostatic coupled ocean atmosphere models could clarify the roles of potential mode drivers, and should be pursued.

Regarding oscillations in Monterey Harbor, we present the first high resolution analysis resolving spectral components to periods as short as 12 s. The spectral nature of these modes indicate they represent a continuum of harmonic oscillators closely spaced in wavenumber. For example, the 112 s dominant mode can be attributed to standing waves between the tide gauge and multiple boundaries including the rocky coast to the east, the breakwater to the north and mooring docks to the northeast, while the 41 s mode is associated with the breakwater to the south. Concerning wave forcing, it is demonstrated that the primary Harbor mode amplitude grows as the square

OSD
11, 2569–2606, 2014

root of offshore significant wave height, and that there is a mode-specific dependence on wave-arrival direction. It is also observed that tidal phase serves to frequency modulate the Harbor modes with evidence of enhanced mode energy during high tide.

A temporal analysis monitoring the evolution of Harbor modes in response to wave forcing supports the idea that amplitude modulation of specific Harbor modes arises from modal interference, and it is observed that when such modulations synchronize they can have a significant impact on water level amplitude. Identification of specific modes with associated physical sources raises the possibility of engineering solutions to mitigate specific oscillations. For example, addition of wave energy dissipation structures to the rocky coast and northern breakwater has potential to reduce the dominant Harbor oscillation.

Appendix

The maximal overlap discrete wavelet transform (MODWT Percival and Walden, 2006) is defined by

$$\boldsymbol{X} = \sum_{j}^{J} \mathbf{D}_j + \mathbf{S}_J \tag{1}$$

where $\boldsymbol{X}$ is a time series of length N and j represents a distinct wavelet level. The $\mathbf{D}_j$ are referred to as wavelet details, and $\mathbf{S}_J$ the smooth, each a vector of length N. The details capture transient and oscillatory behavior at different timescales, the smooth are the residual energy not captured by the details and in the optimal decomposition correspond to a moving average of the signal. Each wavelet level is computed with a matrix transform $\mathbf{D}_j = \mathbf{W}_j^T \boldsymbol{\Phi}_j$ and $\mathbf{S}_J = \mathbf{V}_j^T \boldsymbol{\Psi}_J$ where $\mathbf{W}$ and $\mathbf{V}$ are $N \times N$ matrices of MODWT coefficients, $\boldsymbol{\Phi}$ and $\boldsymbol{\Psi}$ are referred to as the wavelet coefficient and scaling coefficient vectors respectively. The wavelet and scaling coefficients are the result of cascaded high-pass (h) or low-pass (g) wavelet and scaling filters recursively applied

OSD
11, 2569–2606, 2014

to the input: $\mathbf{\Phi}_{j,t} = \sum_{l=0}^{L_j-1} h_{j,l} \boldsymbol{X}_{t-1,\mathrm{mod}\,N}$, or $\mathbf{\Psi}_{j,t} = \sum_{l=0}^{L_j-1} g_{j,l} \boldsymbol{X}_{t-1,\mathrm{mod}\,N}$, where the filter width at each level $L_j = (2^j - 1)(L - 1) + 1$ is determined by the length of the mother wavelet L. In terms of the MODWT matrix and wavelet\scaling coefficients the input can then be represented as:

$$\boldsymbol{X} = \sum_{j}^{J} \mathbf{W}_j^T \mathbf{\Phi}_j + \mathbf{V}_J^T \mathbf{\Psi}_J. \tag{2}$$

The MODWT provides a convenient encapsulation of the signal energy in terms of the wavelet and scaling coefficient vectors:

$$\|\boldsymbol{X}\|^2 = \sum_{j}^{J} \|\mathbf{\Phi}_j\|^2 + \|\mathbf{\Psi}_J\|^2. \tag{3}$$

which is related to the sample variance of $\boldsymbol{X}$. It is useful to plot the wavelet coefficients of each level scaled by its respective magnitude squared so that the relative amplitude scales represent the partial variance contributed by each level.

Acknowledgements. The authors gratefully acknowledge insightful discussions and reviews of the manuscript by Laurence Breaker of Moss Landing Marine Laboratory, University of California, and Yu-Heng Tseng, National Center for Atmospheric Research (NCAR) Earth Systems Laboratory.

References

AMS: Seiches in Lake Garda, Mon. Weather Rev., 31, 532–533, doi:10.1175/1520-0493(1903)31[532b:SILG]2.0.CO;2, 1903. 2570

AMS: The seiche and its mechanical explanation, Mon. Weather Rev., 34, 226, doi:10.1175/1520-0493(1906)34<226b:TSAIME>2.0.CO;2, 1906. 2570

OSD
11, 2569–2606, 2014

Bloomfield, P.: Fourier Analysis of Time Series: An Introduction, Wiley, New York, 1st Edn., 1976. 2574
Breaker, L. C., Broenkow, W. W., Watson, W. E., and Jo, Y.: Tidal and non-tidal oscillations in Elhorn Slough, California, Estuar. Coast., 31, 239–257, 2008. 2571, 2585
Breaker, L. C., Tseng, Y., and Wang, X.: On the natural oscillations of Monterey Bay: observations, modeling, and origins, Prog. Oceanogr., 86, 380–395, doi:10.1016/j.pocean.2010.06.001, 2010. 2572, 2579, 2580, 2586
Bromirski, P. D. and Duennebier, F. K.: The near-coastal microseism spectrum: spatial and temporal wave climate relationships, J. Geophys. Res.-Sol. Ea., 107, ESE 5-1–ESE 5-20, doi:10.1029/2001JB000265, 2002. 2582
Carter, G. S. and Gregg, M. C.: Intense, variable mixing near the head of Monterey Submarine Canyon, J. Phys. Oceanogr., 32, 3145–3165, doi:10.1175/1520-0485(2002)032<3145:IVMNTH>2.0.CO;2, 2002. 2571, 2580, 2582, 2583
CDIP: Station 156 Monterey Canyon Outer, available at: http://cdip.ucsd.edu/?nav=recent&stn=156&sub=observed&xitem=info&stream=p1, last access: 14 November 2014. 2573
Chrystal, G.: On the hydrodynamical theory of seiches, T. Roy. Soc. Edin.-Earth, 41, 599–649, doi:10.1017/S0080456800035523, 1906. 2570
Darwin, G. H.: The Tides and Kindred Phenomena in the Solar System, Houghton, Boston, 1899. 2570
Forston, E. P., Brown, F. R., Hudson, R. Y., Wilson, H. B., and Bell, H. A.: Wave and surge action, Monterey Harbor, Monterey California, Tech. Rep. 2-301, United States Army Corps of Engineers, Waterways Experiment Station, Vicksburg, MS, 45 Plates, 1949. 2571
Gill, A. E.: Atmosphere-Ocean Dynamics, Academic Press, New York, 1982. 2585
Hasselmann, K.: A statistical analysis of the generation of microseisms, Rev. Geophys., 1, 177–210, doi:10.1029/RG001i002p00177, 1963. 2582
IOOS: A National Operational Wave Observation Plan. Integrated Ocean Observing System (IOOS) plan for a surface-wave monitoring network for the United States, Tech. rep., Integrated Ocean Observing System, available at: http://www.ioos.noaa.gov/library/wave_plan_final_03122009.pdf (last access: 14 November 2014), 2009. 2574
Kedar, S., Longuet-Higgins, M., Webb, F., Graham, N., Clayton, R., and Jones, C.: The origin of deep ocean microseisms in the North Atlantic Ocean, P. R. Soc. A, 464, 777–793, doi:10.1098/rspa.2007.0277, 2008. 2580

OSD
11, 2569–2606, 2014

Key, S. A.: Internal tidal bores in the Monterey Canyon, M. S. thesis, Naval Postgraduate School, available at: http://www.dtic.mil/dtic/tr/fulltext/u2/a370949.pdf (last access; 14 November 2014), 1999. 2570, 2580, 2582

Kundu, P. K.: Fluid Mechanics, Academic Press, San Diego, 1st Edn., 1990. 2584

Kunze, E., Rosenfeld, L. K., Carter, G. S., and Gregg, M. C.: Internal waves in Monterey Submarine Canyon, J. Phys. Oceanogr., 32, 1890–1913, doi:10.1175/1520-0485(2002)032<1890:IWIMSC>2.0.CO;2, 2002. 2570, 2580, 2582, 2583

NOAA: Monterey, CA, National Water Level Observation Network – Station ID: 9413450, available at: http://tidesandcurrents.noaa.gov/stationhome.html?id=9413450, last access: 14 November 2014a. 2573

NOAA: Harmonic Constituents for 9413450, Monterey CA, available at: http://tidesandcurrents.noaa.gov/harcon.html?id=9413450, last access: 14 November 2014b. 2573

Park, J., Heitsenrether, R., and Sweet, W.: Microwave and acoustic water level and significant wave height estimates at NOAA tide stations, J. Atmos. Ocean. Tech., 31, 2294–2308, 2014. 2574

Parke, M. E. and Gill, S. K.: On the sea state dependence of sea level measurements at platform Harvest, Mar. Geod., 18, 105–111, 1995. 2574

Percival, D. B. and Walden, A. T.: Wavelet Methods for Time Series Analysis, Cambridge University Press, New York, 2006. 2577, 2587

Petruncio, E., Rosenfeld, L., and Paduan, P.: Observations of the internal tide in Monterey Canyon, J. Phys. Oceanogr., 28, 1873–1903, doi:10.1175/1520-0485(1998)028<1873:OOTITI>2.0.CO;2, 1998. 2570

Raines, W. A.: Sub-tidal oscillations in Monterey Harbor, M. S. thesis, Naval Postgraduate School, available at: https://calhoun.nps.edu/bitstream/handle/10945/13214/subtidaloscillat00bain.pdf?sequence=1 (last access: 14 November 2014), 1967. 2571

Rosenfeld, L. K., Schwing, F. B., Garfield, N., and Tracy, D. E.: Bifurcated flow from an upwelling center: a cold water source for Monterey Bay, Cont. Shelf. Res., 14, 931–964, doi:10.1016/0278-4343(94)90058-2, 1994. 2571, 2585

Shchepetkin, A. F. and McWilliams, J. C.: The regional oceanic modeling system (ROMS): a split-explicit, free-surface, topography-following-coordinate oceanic model, Ocean Model., 9, 347–404, doi:10.1016/j.ocemod.2004.08.002, 2005. 2580

Strub, P. T., Kosro, P. M., and Huyer, A.: The nature of the cold filaments in the California Current system, J. Geophys. Res.-Oceans, 96, 14743–14768, doi:10.1029/91JC01024, 1991. 2571

OSD
11, 2569–2606, 2014

Tseng, Y.-H. and Breaker, L. C.: Nonhydrostatic simulations of the regional circulation in the Monterey Bay area, J. Geophys. Res.-Oceans, 112, C12017, doi:10.1029/2007JC004093, 2007. 2571, 2583, 2584, 2585

Tseng, Y.-H., Dietrich, D. E., and Ferziger, J. H.: Regional circulation of the Monterey Bay region: hydrostatic versus nonhydrostatic modeling, J. Geophys. Res.-Oceans, 110, C09015, doi:10.1029/2003JC002153, 2005. 2571

Tseng, Y.-H., Chien, S.-H., Jin, J., and Miller, N. L.: Modeling air-land-sea interactions using the integrated regional model system in Monterey Bay, California, Mon. Weather Rev., 140, 1285–1306, doi:10.1175/MWR-D-10-05071.1, 2012. 2571, 2583

Waxler, R. and Gilbert, K. E.: The radiation of atmospheric microbaroms by ocean waves, J. Acoust. Soc. Am., 119, 2651–2664, doi:10.1121/1.2191607, 2006. 2581

Webb, S. C. and Cox, C. S.: Observations and modeling of seafloor microseisms, J. Geophys. Res.-Sol. Ea., 91, 7343–7358, doi:10.1029/JB091iB07p07343, 1986. 2581, 2582

Wilson, B. W., Hendrickson, J. A., and Kilmer, R. E.: Feasibility study for a surge-action model of Monterey Harbor, California, Tech. Rep. 2-136, United States Army Corps of Engineers, Waterways Experiment Station, Vicksburg, MS, 1965. 2571, 2576, 2579

OSD
11, 2569–2606, 2014

Table 1. Spatial scales of the Bay, Bight and Harbor modes according to the dispersion relation $\omega^2 = g\,k\tanh(k\,d)$ where ω is frequency, k the wavenumber, d the water depth and λ the wavelength. The Bay and Bight modes use depths of 60 m, the Harbor modes 7.5 m.

Bay		Bight		Harbor	
Period (min)	$\lambda/2$ (km)	Period (min)	$\lambda/2$ (km)	Period (s)	$\lambda/2$ (m)
55.9	40.7	10.1	7.4	112	480
36.7	26.7	9.0	6.5	60	252
27.4	19.9	4.2	3.1	41	172
21.7	15.8			31	133
18.4	13.4			16	67
16.5	12.0			12	50

OSD
11, 2569–2606, 2014

Table 2. Wavelet level dominant periods in seconds.

Level	9/20 22:00–24:00 UTC H_s 0.8–1.1 (m)	9/21 16:00–18:00 UTC H_s 2.4 (m)	10/4 10:00–12:00 UTC H_s 2.0 (m)
W2	13	12	9
W3	15	14	12
W4	31	31	30
W5	60	58	61
W6	96	101	111
W7	126	117	118
W8	486	405	260
W9	729	663	911
W10	800	830	800
W11	1030	1090	1285

OSD
11, 2569–2606, 2014

Table 3. Mean water level spectral amplitudes at the Bay-wide oscillation modes estimated from 1 Hz nontide residuals over 63 days. The 95 % confidence interval on spectral amplitude is 3.0 dB.

Period (min)	PSD dB ($m^2\,Hz^{-1}$)	ΔdB ($m^2\,Hz^{-1}$)	Water Level (m)
36.7	−9.3	0.0	0.341
27.4	−12.8	−3.4	0.230
55.9	−13.3	−4.0	0.215
21.7	−15.7	−6.4	0.164
18.4	−17.8	−8.4	0.129
16.5	−17.9	−8.5	0.128

OSD
11, 2569–2606, 2014

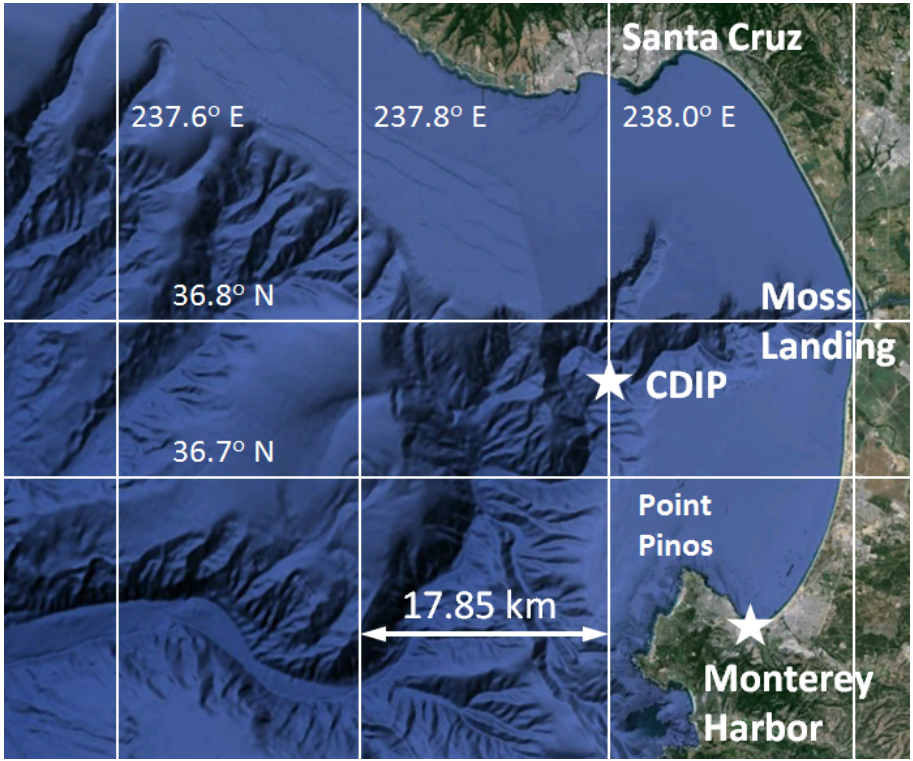

Figure 1. Monterey Bay and Canyon. The location of the wave gauge (CDIP) and water level gauges are indicated with stars.

OSD
11, 2569–2606, 2014

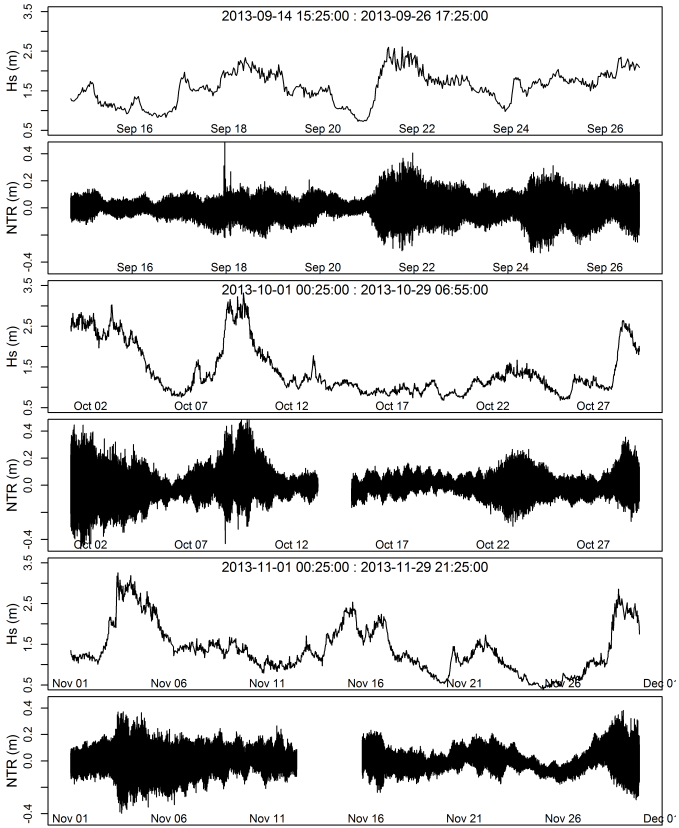

Figure 2. Significant wave height (H_s) at the Monterey Canyon CDIP buoy (30 min data) and 1 Hz nontide residual water (NTR) levels from the NOAA tide gauge in Monterey Harbor.

OSD
11, 2569–2606, 2014

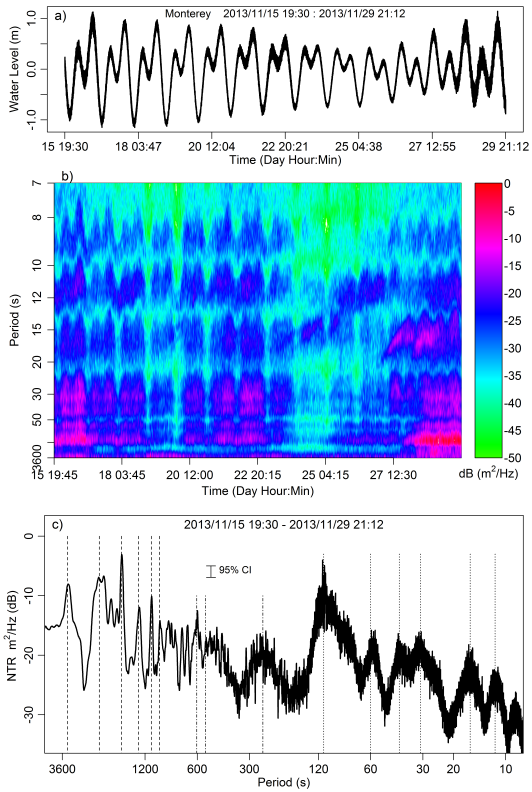

Figure 3. (a) Raw 1 Hz water levels from 15 November 2013 through 29 November 2013. **(b)** Spectrogram of the water levels. **(c)** Power spectral density estimates of nontide residual water levels. Dashed vertical lines mark the Bay-wide resonance modes (55.9, 36.7, 27.4, 21.8, 18.5 and 16.5 min), dash-dot lines mark Bight periods (10.1, 9.0 and 4.2 min) and dotted lines the Harbor modes (112, 60, 41, 31, 16 and 12 s).

OSD
11, 2569–2606, 2014

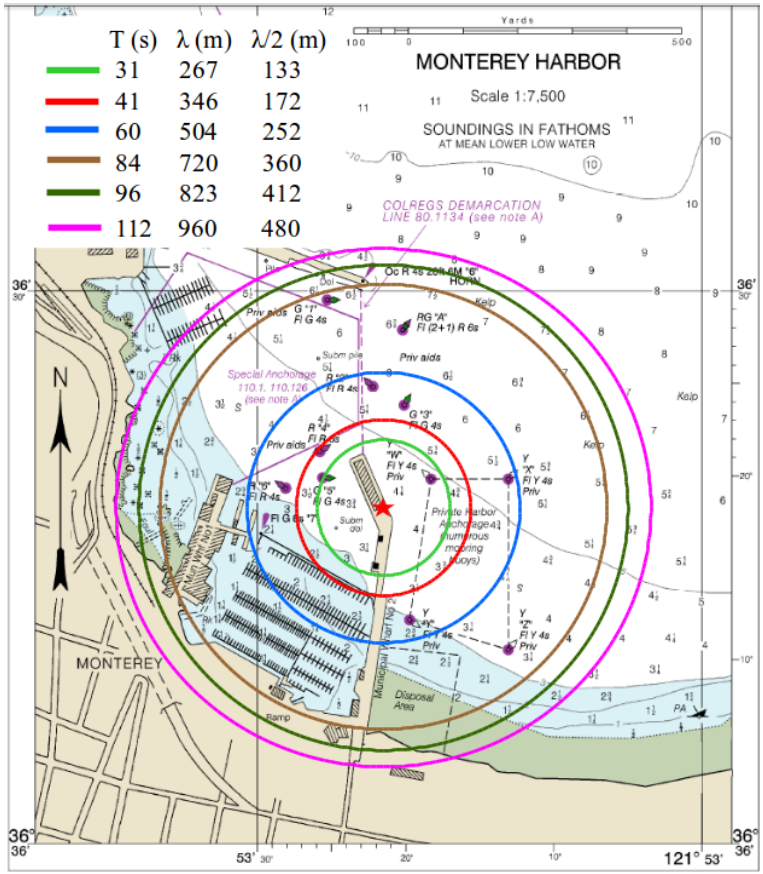

Figure 4. Chart of Monterey Harbor with circles of radius $\lambda/2$ centered on the water level gauge corresponding to waves with periods at the fundamental modes observed in the power spectra. Wavelengths are determined from the general dispersion relation applied at a depth of 7.5 m.

OSD
11, 2569–2606, 2014

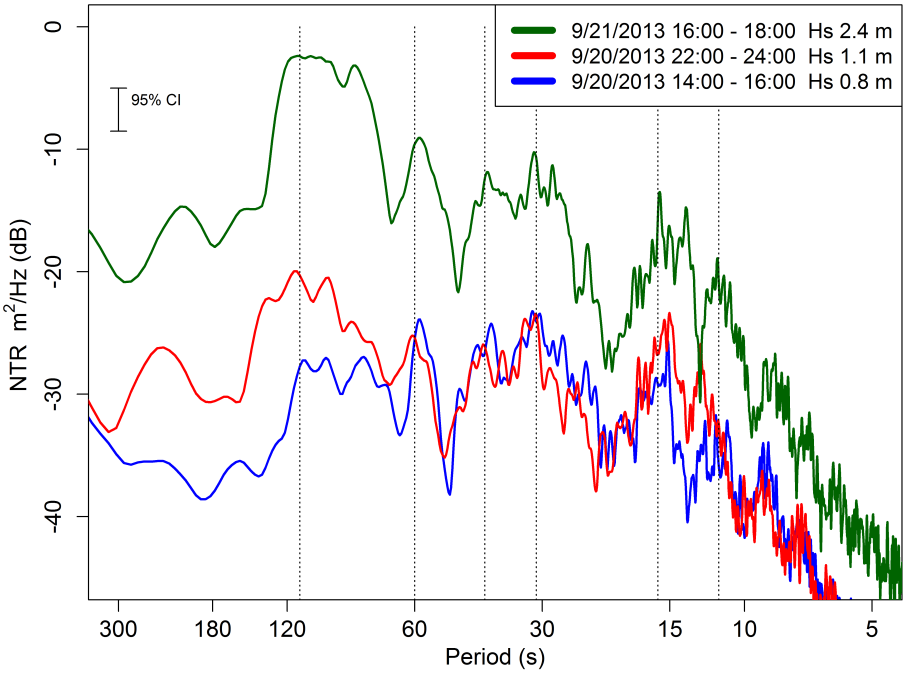

Figure 5. Power spectral density estimates of 1 Hz nontide residual over 2 h periods during 20 and 21 September 2013 with different deep water wave heights. Dotted vertical lines mark the Harbor modes at 112, 60, 41, 31, 16 and 12 s.

OSD
11, 2569–2606, 2014

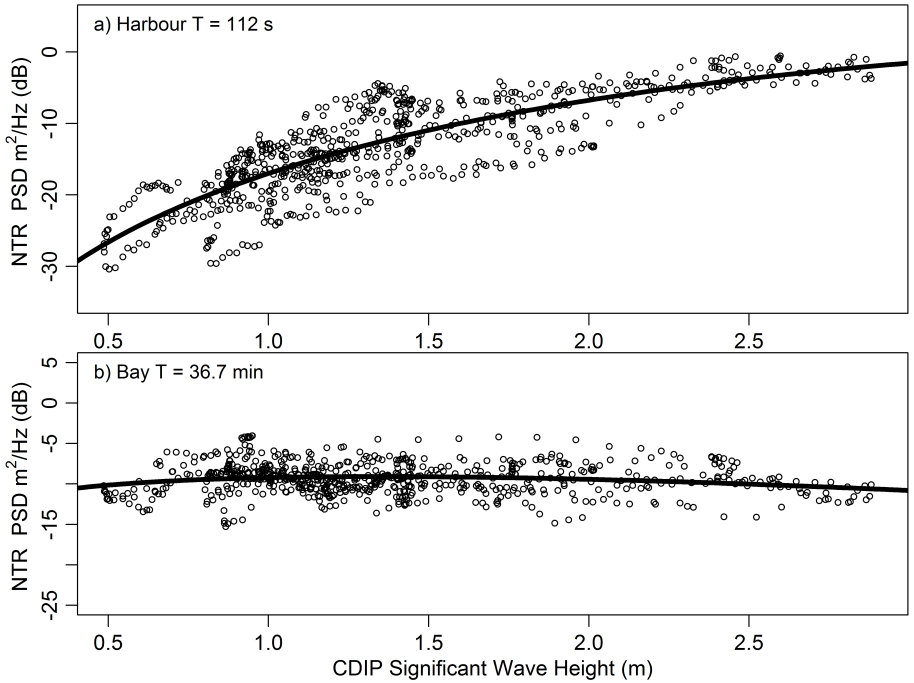

Figure 6. (a) Water level amplitudes at the dominant Harbor period of 112 s, and, **(b)** amplitudes at the dominant Bay period of 36.7 min as a function of significant wave height. Each amplitude is estimated from a PSD computed over an 18 h moving window with a time increment of 1 h. Solid lines are a least squares fit to a nonlinear model ($PSD_M = \alpha H_s + \beta H_s^{1/2}$). Note that the water level amplitudes are in dB.

OSD
11, 2569–2606, 2014

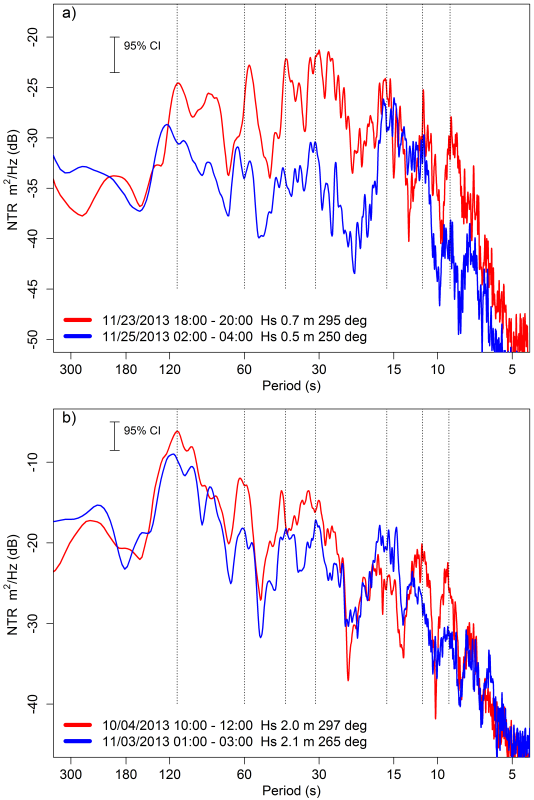

Figure 7. (a) Power spectral density estimates of 1 Hz nontide residual water level over 2 h periods with offshore significant wave heights of 0.5 and 0.7 m and arrival directions of 250 and 295°. **(b)** Power spectral density estimates of 1 Hz nontide residual water level over 2 h periods with offshore significant wave heights of 2.0 and 2.1 m and arrival directions of 265 and 297°. Dotted lines correspond to Harbor modes (112, 60, 41, 31, 16 and 9 s).

OSD
11, 2569–2606, 2014

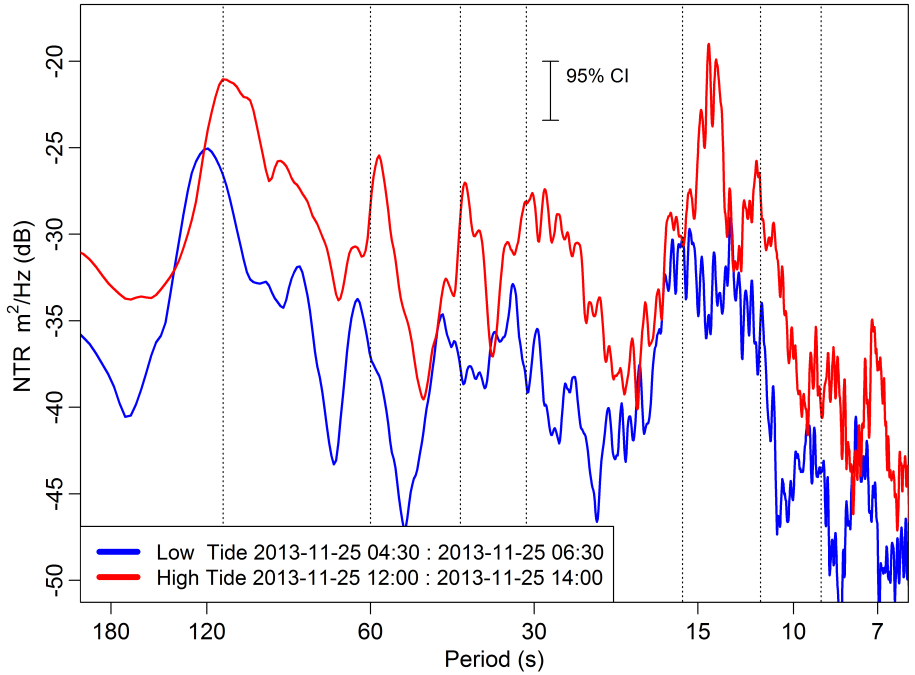

Figure 8. PSD estimates of 1 Hz NTR data from 2 h periods centered on low and high water of a tidal period. Offshore waves were low during this period. Dotted vertical lines mark Harbor modes at 112, 60, 41, 31, 16 and 12 s.

OSD
11, 2569–2606, 2014

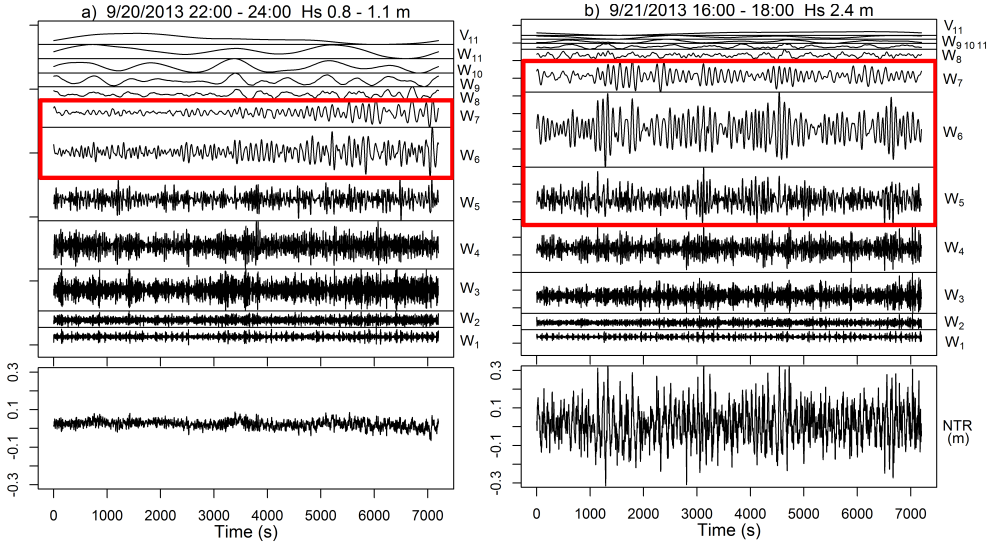

Figure 9. (a) Discrete wavelet transform decomposition of nontide residual during a 2 h period when deep water significant wave height increased from 0.8 to 1.1 m. The red box highlights the W_6 and W_7 wavelet levels exhibiting emergence of energy in these two bands as wave height increases. **(b)** Discrete wavelet transform decomposition of nontide residual during a 2 h period when deep water significant wave height was 2.4 m. The red box highlights the W_5, W_6 and W_7 wavelet levels exhibiting dominance of energy in these bands and amplitude modulation. Power spectral density estimates of these 2 h period are shown in Fig. 5.

OSD
11, 2569–2606, 2014

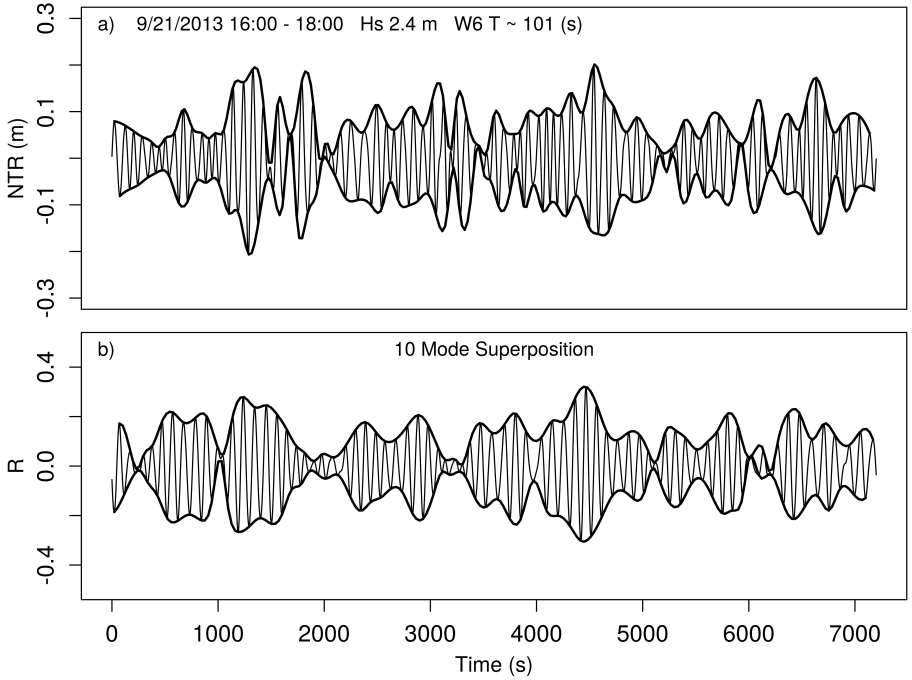

Figure 10. (a) Wavelet level W_6 of the nontide residual over a 2 h period on 21 September 2013 when offshore wave height was 2.4 m. **(b)** Time series reconstruction from ten spectral amplitudes of Fig. 5 at periods of 58, 83, 94, 97, 100, 104, 107, 112 116 and 209 s.

OSD
11, 2569–2606, 2014

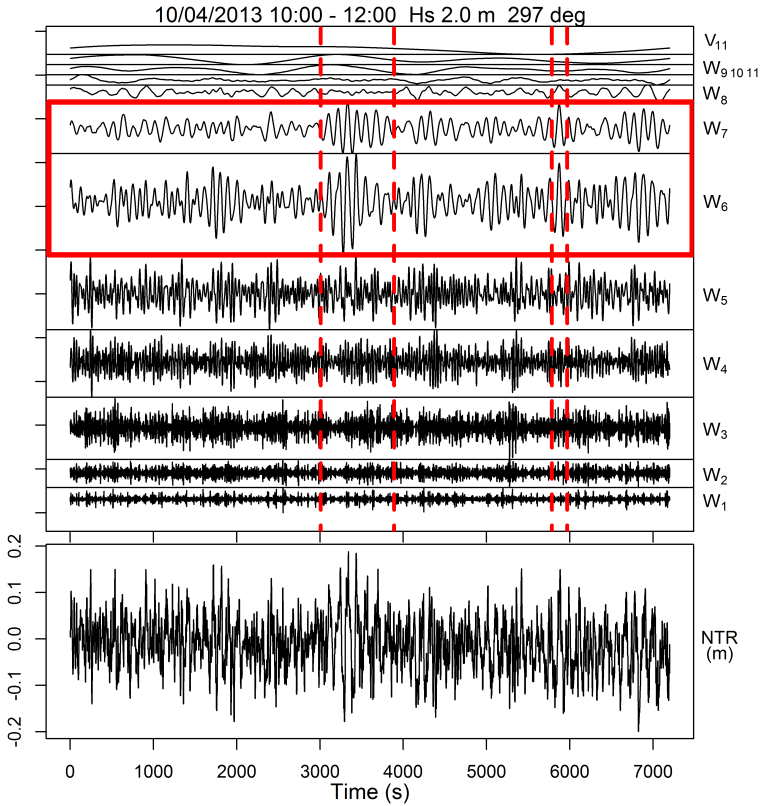

Figure 11. Discrete wavelet transform decomposition of nontide residual water level during a 2 h period with offshore significant wave height of 2.0 m. Dashed vertical lines mark periods of synchronization between the W_7 ($T \approx 118$ s) and W_6 ($T \approx 111$ s) levels.

OSD
11, 2569–2606, 2014

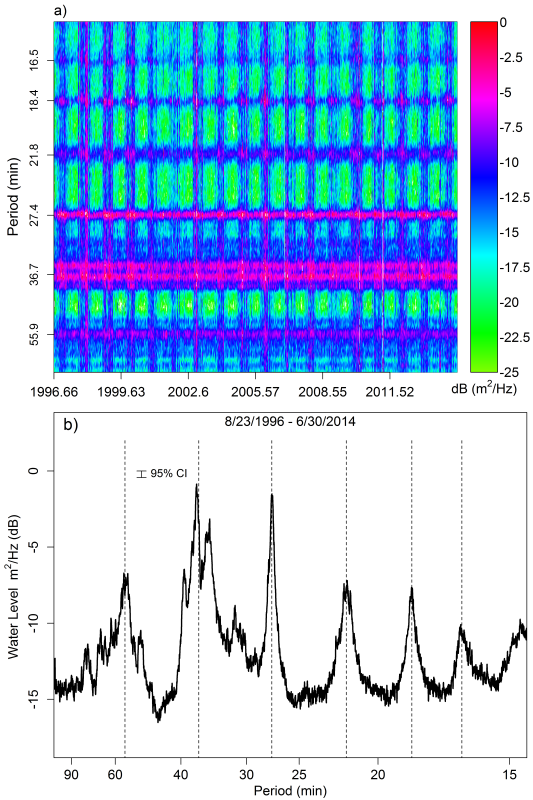

Figure 12. (a) Spectrogram of 6 min water levels at the Monterey tide gauge from August 1996 through June 2014. **(b)** Power spectral density estimate of 6 min water levels at the Monterey tide gauge from August 1996 through June 2014. Dashed vertical lines mark the Bay-wide resonance modes of 55.9, 36.7, 27.4, 21.8, 18.5 and 16.5 min.

OSD
11, 2569–2606, 2014